On the Structure and Chemical Bonding of Tri-Tungsten Oxide Clusters $W_3O_n^-$ and W_3O_n ($n = 7-10$): W_3O_8 As A Potential Molecular Model for O-Deficient Defect Sites in Tungsten Oxides

Xin Huang,[†] Hua-Jin Zhai,[†] Jun Li,[‡] and Lai-Sheng Wang*[,†]

Department of Physics, Washington State University, 2710 University Drive, Richland, Washington 99354, and W. R. Wiley Environmental Molecular Sciences Laboratory and Chemical Sciences Division, Pacific Northwest National Laboratory, P.O. Box 999, Richland, Washington 99352

Received: September 19, 2005; In Final Form: November 8, 2005

Electronic and structural properties of a series of tri-tungsten oxide clusters, $W_3O_n^-$ and W_3O_n ($n = 7-10$), are investigated using photoelectron spectroscopy and density functional theory (DFT) calculations. Both W 5d and O 2p detachment features are observed for $n = 7-9$, whereas only detachment features from O 2p-type orbitals are observed for $W_3O_{10}^-$ at high electron binding energies (>7 eV). A large energy gap (~3.4 eV) is observed for the stoichiometric W_3O_9 cluster, which already reaches the bulk value, suggesting that W_3O_9 can be viewed as the smallest molecular model for bulk WO_3. DFT calculations are carried out to locate the most stable structures for both the anion and neutral clusters; time-dependent DFT method is used to predict the vertical detachment energies and to compare with the experimental data. It is shown that W_3O_9 possesses a D_{3h} structure, in which each W atom is tetrahedrally coordinated with two bridging O atoms and two terminal O atoms. W_3O_8 and W_3O_7 can be viewed as removing one and two terminal O atoms from W_3O_9, respectively, whereas W_3O_{10} can be viewed as replacing a terminal O in W_3O_9 by a peroxo O_2 unit. We show that W_3O_8 contains a localized W^{4+} site, which can readily react with O_2 to form the W_3O_{10} clusters with a calculated O_2 adsorption energy of −78 kcal/mol. It is suggested that the W_3O_8 cluster can be viewed as a molecular model for O-deficient site in tungsten oxides.

1. Introduction

Tungsten oxides have many industrial applications[1−4] and are important acid−base and redox catalysts.[5−11] However, the identification of active sites in metal oxide catalysts has been very difficult. Gas-phase cluster studies have been considered as an alternative approach to obtain fundamental insight into the complicated structures and chemical processes in oxide materials and catalysts.[12−21] Interest in transition-metal oxide clusters has been motivated in particular by the use of these species to aid the elucidation of the mechanisms of catalytic reactions.[22,23] Gas-phase studies, coupled with state-of-the-art theoretical calculations, can provide molecular level insight into the nature of active species in catalysis.[13,14] As a first step in developing a comprehensive understanding of complex catalytic processes on early transition-metal oxides, we are interested in systematic studies of the electronic structure and chemical bonding of size-selected tungsten oxide clusters. Recently, we have reported joint experimental and theoretical investigations on a variety of tungsten oxide clusters.[21,24,25] To mimic the geometric and electronic properties of tungsten oxide surfaces and defects, relatively large W_mO_n clusters are of interest. In the present work, we investigate the electronic structure and chemical bonding of the tri-tungsten oxide clusters, $W_3O_n^-$ and W_3O_n ($n = 7-10$), which include the stoichiometric W_3O_9 cluster and both O-deficient (W_3O_7 and W_3O_8) and O-rich (W_3O_{10}) clusters.

There have been relatively few reports on tri-tungsten oxide clusters,[26−28] and very little is known about tri-tungsten oxide species, except W_3O_9. Early mass-spectrometric studies[26,27] indicated that the vapor of tungsten trioxide consists mainly of the stoichiometric molecule W_3O_9. Weltner et al.[28] performed a matrix infrared spectroscopic study on tungsten oxide clusters and tentatively assigned certain infrared bands to W_3O_8/W_3O_9 on the basis of their intensity variations with vaporization conditions. Sun et al.[29] recently reported the photoelectron spectrum of $W_3O_9^-$ at 193 nm together with other stoichiometric $W_nO_{3n}^-$ ($n = 1, 2, 4$) clusters. They also presented the optimized structures of W_3O_9 and $W_3O_9^-$ at the BPW91 level.

We have obtained photoelectron spectra of $W_3O_n^-$ ($n = 7-10$) at 157 nm (7.866 eV). The high photon energy is necessary because of the relatively high electron binding energies of the oxide cluster anions, in particular, the O-rich species. A large energy gap was observed for $W_3O_9^-$, consistent with a stable stoichiometric W_3O_9 molecule, in which W reaches its highest oxidation state (W^{6+}). Lower binding energy features due to excess 5d electrons were observed for the O-deficient clusters, whereas high electron binding energies were observed for the O-rich $W_3O_{10}^-$ cluster. Extensive density functional theory (DFT) calculations were performed to elucidate the structures and bonding in the tri-tungsten oxide clusters in both the neutral and anionic species, W_3O_n and $W_3O_n^-$ ($n = 7-10$). In particular, the ground state of W_3O_8 is found to be an interesting species, which may be viewed as a model for O-deficient defect sites. The ground state of W_3O_{10} is found to be a peroxo complex, which can be viewed to be formed from

* To whom correspondence should be addressed. E-mail: ls.wang@pnl.gov.
[†] Washington State University and Pacific Northwest National Laboratory.
[‡] Pacific Northwest National Laboratory.

10.1021/jp055325m CCC: $33.50
Published on Web 12/15/2005

chemisorption of O_2 on W_3O_8 and may serve as important intermediate in catalytic oxidation reactions.

2. Experimental and Theoretical Methods

2.1. Photoelectron Spectroscopy. The experiments were carried out using a magnetic-bottle photoelectron spectroscopy (PES) apparatus equipped with a laser vaporization supersonic cluster source.[30,31] Briefly, $W_mO_n^-$ cluster anions were produced by laser vaporization of a pure tungsten target in the presence of helium carrier gas seeded with 0.5% O_2 and were analyzed using a time-of-flight mass spectrometer. The $W_3O_n^-$ (n = 7−10) clusters of current interest were each mass selected and decelerated before being photodetached with 157-nm photons from an F_2 excimer laser. Photoelectrons were collected at nearly 100% efficiency by the magnetic bottle and analyzed in a 3.5 m long electron flight tube. Photoelectron spectra were calibrated using the known spectrum of Rh^-, and the energy resolution of the apparatus was $\Delta E_k/E_k \approx 2.5\%$, that is, ~25 meV for 1 eV electrons.

2.2. Density Functional Calculations. The theoretical calculations were performed at the DFT level using the B3LYP hybrid functional.[32−34] A number of structural candidates were evaluated, and the search for the global minima was performed using analytical gradients with the Stuttgart 14-valence-electron pseudopotentials and the valence basis sets[35,36] augmented with two f-type and one g-type polarization functions [ζ(f) = 0.256, 0.825; ζ(g) = 0.627] for tungsten as recommended by Martin and Sundermann[37] and the aug-cc-pVTZ basis set for oxygen.[38,39] Scalar relativistic effects, i.e., the mass-velocity and Darwin effects, were taken into account via the quasirelativistic pseudopotentials. Since we were mainly interested in explaining the experimentally observed PES spectra, no further effort was devoted to resolve the spin−orbit coupled fine structures in the calculated spectra. Our previous results on tungsten oxides showed that spin−orbit coupling effects would shift the orbital energies by up to a few tenth of an eV, which would not affect the spectral assignment.[40] Only a selected set of optimized structures (the ground state and a few low-lying isomers), considered to be important in interpreting the experimental data, are reported. Vibrational frequency calculations were performed at the same level of theory to verify the nature of the stationary points. The vertical detachment energies (VDEs) were calculated using a combined ΔSCF-TDDFT approach, as we previously outlined.[41,42] In this approach, the ground-state energies of the anions and the neutrals were calculated from the ΔSCF energy difference at the B3LYP level, whereas the excited states of the one-electron-detached species were obtained from TDDFT calculations of the neutrals. For all calculations, the extra fine integration grid was used to obtain highly accurate DFT results. All calculations were accomplished using the NWChem 4.6 program and the Molecular Science Computing Facility located at the Environmental Molecular Sciences Laboratory.[43] The Extensible Computational Chemistry Environment software was used to generate the three-dimensional contours of the calculated Kohn−Sham orbitals.[44]

3. Experimental Results

The PES spectra of $W_3O_n^-$ (n = 7−10) measured at 157 nm are shown in Figure 1. The observed spectral bands are labeled with letters (X, A, B, C). The low binding energy features in $W_3O_n^-$ (n = 7−9) are expanded to illustrate the spectral details. The obtained VDEs and ground-state adiabatic detachment energies (ADEs) are given in Table 1.

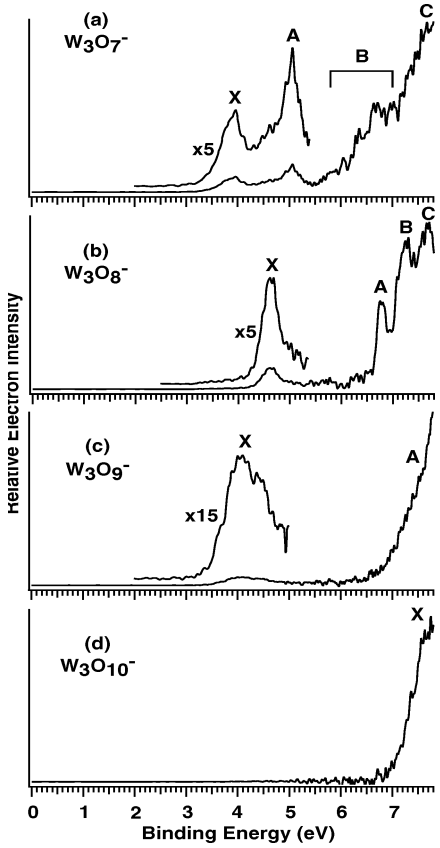

Figure 1. Photoelectron spectra of $W_3O_n^-$ (n = 7−10) at 157 nm (7.866 eV).

The spectrum of $W_3O_7^-$ (Figure 1a) shows two relatively weak bands (X and A) at low binding energies. More intense signals above 6 eV appear to be congested and continuous. The ground-state band X has a VDE of 3.9 eV with a long tail down to ~3.3 eV either due to vibrational hot bands or a large geometry change between the anion and neutral ground states. The ADE of the X band was estimated to be 3.5 ± 0.1 eV, which defines the electron affinity (EA) of neutral W_3O_7. The large uncertainty was a result of the low energy tail, which made it difficult to define the ADE. Band A with a VDE of 5.04 eV is relatively sharp, which should correspond to the first excited state of W_3O_7. A shoulder seems to be present at the lower binding energy side of band A. The spectrum beyond ~6.0 is featureless, which is labeled with B and C simply to denote two spectral regions.

The spectrum of $W_3O_8^-$ (Figure 1b) displays relatively sharp features. A weak band X with a VDE of 4.62 eV is followed by a large energy gap and three well-defined spectral features (A, B, C) at high binding energies. The ground-state band X yields an ADE of 4.37 eV, which defines the EA of neutral W_3O_8. The first excited-state band (A) at a VDE of 6.78 eV gives a X−A gap of 2.16 eV. The VDEs of bands B and C are measured to be 7.23 and 7.65 eV, respectively.

The PES spectrum of the stoichiometric $W_3O_9^-$ cluster is shown in Figure 1c. The ground-state X has weak intensity and is very broad, suggesting a large geometry change between the anion and neutral ground state. The X band yields a VDE of 4.2 eV and an ADE of 3.55 eV. The X band is followed by a large energy gap and the first excited-state band (A) is located at a high binding energy with an estimated onset of ~7 eV. No distinct features were observed in the higher binding energy

TABLE 1: Experimental VDEs of $W_3O_n^-$ ($n = 7-10$) and Comparison with Theoretical VDEs Calculated from the Lowest-Energy Anions (All Energies Are in eV)

		exptl[a]		theor[b,c]			
		ADE	VDE	MO	VDE	MO	VDE
$W_3O_7^-$	X	~3.5	~3.9			29a′ (α)	4.01 (S)
	A		5.04 (5)	28a′ (β)	5.04 (T)		
	B		~6.0−7.0	27a′ (β)	6.40 (T)	28a′ (α)	6.23 (S)
				21a″ (β)	6.65 (T)	27a′ (α)	6.76 (S)
				26a′ (β)	6.74 (T)	21a″ (α)	6.84 (S)
						26a′ (α)	6.90 (S)
	C		>7.0	20a″ (β)	7.42 (T)	20a″ (α)	7.57 (S)
				25a′ (β)	7.57 (T)	25a′ (α)	7.78 (S)
$W_3O_8^-$	X	4.37 (5)	4.62 (5)			$19a_1$ (α)	4.58 (S)
	A		6.78 (3)	$18a_1$ (β)	6.89 (T)		
	B		7.23 (5)	$7a_2$ (β)	7.09 (T)	$7a_2$ (α)	7.20 (S)
				$12b_1$ (β)	7.11 (T)	$12b_1$(α)	7.23 (S)
				$11b_1$ (β)	7.19 (T)	$11b_1$(α)	7.31 (S)
	C		7.65 (5)	$14b_2$ (β)	7.58 (T)	$18a_1$ (α)	7.59 (S)
				$6a_2$ (β)	7.64 (T)		
$W_3O_9^-$	X	3.55 (10)	~4.2			10a₁′ (α)	4.39 (S)
	A		~7.4	$6a_2$″ (β)	7.18 (T)	$6a_2$″ (α)	7.32 (S)
				7e″ (β)	7.20 (T)	7e″ (α)	7.34 (S)
				12e′(β)	7.66 (T)	12e′ (α)	7.81 (S)
				6e″ (β)	7.70 (T)	6e″ (α)	7.83 (S)
$W_3O_{10}^-$	X	7.1 (1)	7.1−7.8	61a (β)	7.09 (T)	62a (α)	7.90 (S)
				58a (β)	7.45 (T)		
				60a (β)	7.54 (T)		
				57a (β)	7.64 (T)		

[a] Numbers in the parentheses represent experimental uncertainty in the last digits. [b] The ground-state electronic configurations for the anions are: $W_3O_7^-$, $(25a')^2(20a'')^2(26a')^2(21a'')^2(27a')^2(28a')^2(29a')^1$; $W_3O_8^-$, $(6a_2)^2(14b_2)^2(11b_1)^2(12b_1)^2(7a_2)^2(18a_1)^2$ $(19a_1)^1$; $W_3O_9^-$, $(6e'')^4$ $(12e')^4$ $(7e'')^4$ $(6a_2'')^2$ $(10a_1')^1$; $W_3O_{10}^-$, $(57a)^2$ $(58a)^2$ $(59a)^2$ $(60a)^2$ $(61a)^2$ $(62a)^1$. [c] The labels "α" and "β" denote majority and minority spins, whereas S and T denote singlet and triplet W_3O_n final states upon photodetachment.

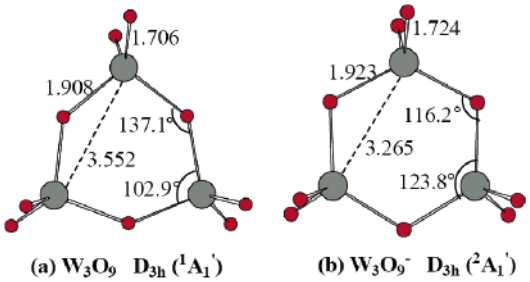

Figure 2. Optimized structures for W_3O_9 and $W_3O_9^-$. The bond lengths are in angstroms and bond angles in degrees.

part of the spectrum. The PES spectrum in Figure 1c yields an approximate energy gap of ~3.4 eV, which is nearly identical to the bulk band gap of WO_3. In the previous work by Sun et al. at 193 nm,[29] only a lower limit for the highest occupied molecular orbital (HOMO)−lowest unoccupied molecular orbital (LUMO) gap was given (>1.5 eV). Clearly the lower photon energy used could not have accessed the band gap.

The $W_3O_{10}^-$ cluster possesses a high electron binding energy and its PES spectrum at 157 nm only gave an onset at 7.1 eV, which yielded a very large EA for neutral W_3O_{10}.

4. Theoretical Results

The optimized ground-state geometries of W_3O_n and $W_3O_n^-$ and selected low-lying isomers are presented in Figures 2−5. We first present the results for the stoichiometric clusters, W_3O_9 and $W_3O_9^-$ (Figure 2), because the O-deficient and O-rich species are related to the stoichiometric clusters. In the following discussion, O_t and O_b stand for the terminal and bridging oxygen atoms, respectively.

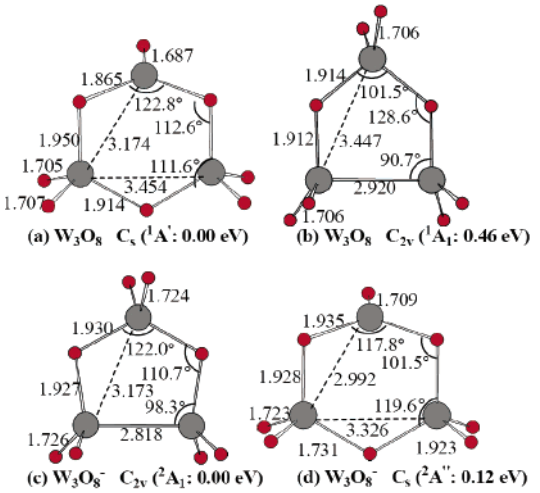

Figure 3. Optimized structures and their relative energies for W_3O_8 and $W_3O_8^-$. The bond lengths are in angstroms and bond angles in degrees.

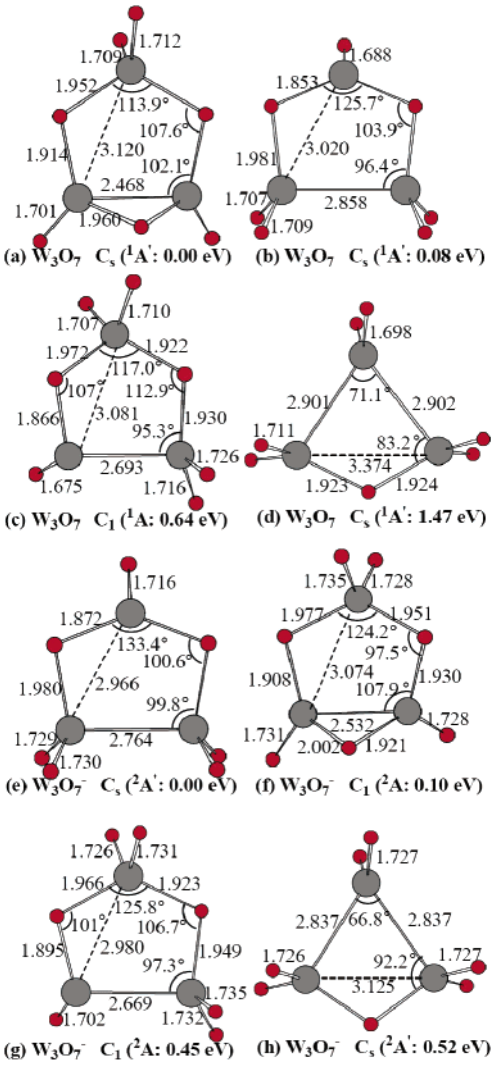

Figure 4. Optimized structures and their relative energies for W_3O_7 and $W_3O_7^-$. The bond lengths are in angstroms and bond angles in degrees.

4.1. Stoichiometric Clusters W_3O_9 and $W_3O_9^-$. The optimized ground-state structures of W_3O_9 and $W_3O_9^-$ are shown in Figure 2. For W_3O_9 neutral, we considered two initial starting geometries with C_{3v} and D_{3h} symmetries, which

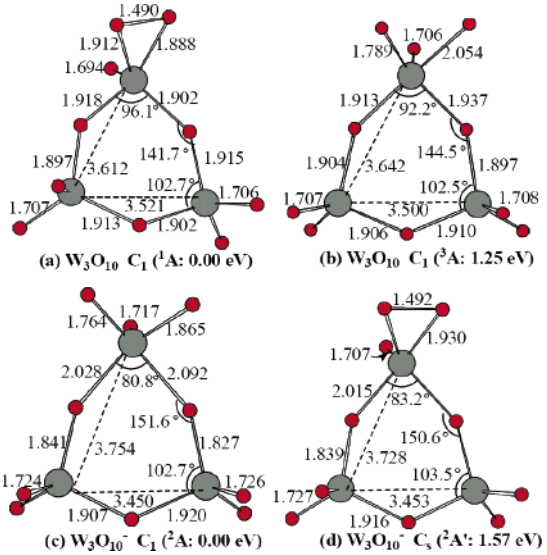

Figure 5. Optimized structures and their relative energies for W_3O_{10} and $W_3O_{10}^-$. The bond lengths are in angstroms and bond angles in degrees.

converged to the same structure. The ground state of W_3O_9 was found to be closed shell with D_{3h} ($^1A_1'$) symmetry. Each tungsten atom is tetrahedrally coordinated with two terminal and two bridging O atoms (Figure 2a). This is basically consistent with that identified by Sun et al.[29] at BPW91, except that the structure of Sun et al. possesses lower symmetry (C_{3v}). The W—O_t and W—O_b bond lengths are 1.706 and 1.908 Å, close to those expected for W═O double and W—O single bonds, respectively. The ∠WO_bW bond angle is 137.1°, much larger than the ∠O_b-WO_b angle of 102.9°.

The ground state of $W_3O_9^-$ was found to be a doublet with D_{3h} ($^2A_1'$) symmetry (Figure 2b), similar to that for the neutral. The W—O_t and W—O_b bond lengths are 1.724 and 1.923 Å, respectively, only slightly longer than those in the neutral species. However, the ∠WO_bW and ∠O_bWO_b bond angles change significantly. The ∠WO_bW bond angle is 116.2°, decreased by about 21° relative to that of neutral W_3O_9, whereas the ∠O_bWO_b bond angle increases by about 21°, so that the W_3O_3 ring is almost a perfect hexagon.[25] This large geometry change between the anion and neutral ground state is consistent with the broad ground-state band observed in the photoelectron spectrum of $W_3O_9^-$ (Figure 1c). It should be mentioned that there are other low-lying isomers for $W_3O_9^-$ that are close in energy to the D_{3h} structure at the DFT level. Further theoretical calculations with more sophisticated methods may be necessary to resolve the true ground state of $W_3O_9^-$.

4.2. Oxygen-Deficient Cluster: W_3O_8 and $W_3O_8^-$. We started the structural searches for the O-deficient clusters by removing O atoms from the ground state of the stoichiometric W_3O_9 cluster. We located two isomers for neutral W_3O_8. The ground state of W_3O_8 was found to be closed shell with C_s ($^1A'$) symmetry (Figure 3a), which can be viewed as removing one terminal O atom from the D_{3h} W_3O_9. The other isomer with C_{2v} ($^1A_1$) symmetry (Figure 3b) is 0.46 eV higher in energy and is derived from removing one bridging O atom from W_3O_9. In the anion, the C_{2v} structure (Figure 3c) was found to be the ground state, becoming more stable than the C_s isomer (Figure 3d) by 0.12 eV. The structures of the two $W_3O_8^-$ isomers are very similar to their corresponding neutrals with very little geometrical changes, consistent with the relatively sharp PES features observed for $W_3O_8^-$ (Figure 1b).

4.3. Oxygen-Deficient Cluster: W_3O_7 and $W_3O_7^-$. We performed an extensive search of the potential energy surfaces of W_3O_7 and $W_3O_7^-$ using the two isomers of W_3O_8 and $W_3O_8^-$ (Figure 3) as our starting points. We were able to locate four low-lying isomers, as shown in Figure 4. The ground state of neutral W_3O_7 is C_s ($^1A'$) (Figure 4a), which is formed from removing two terminal O atoms on two different W sites from the neutral W_3O_9. The second low-lying isomer (Figure 4b) also with C_s symmetry is only 0.08 eV higher in energy and is originated from removing one terminal and one bridging O atom from two different W sites of W_3O_9. The third isomer of W_3O_7 (Figure 4c), 0.64 eV higher in energy, is formed by removing one terminal and one bridging O atom from the same W atom of W_3O_9. The W_3O_7 isomer formed by removing two bridging O atoms from W_3O_9 is much higher in energy by 1.47 eV (Figure 4d).

For the $W_3O_7^-$ anion, the ground state is the dibridged C_s ($^2A'$) structure (Figure 4e), corresponding to the second low-lying isomer of the neutral cluster. The second isomer of $W_3O_7^-$, only 0.10 eV higher in energy, corresponds to the ground state of the neutral. The third (Figure 4g) and fourth (Figure 4h) isomers of the anion are similar to the corresponding neutral isomers and are higher in energy by 0.45 and 0.52 eV above the ground state, respectively.

4.4. Oxygen-Rich Clusters: W_3O_{10} and $W_3O_{10}^-$. We found two isomers each for W_3O_{10} and $W_3O_{10}^-$, as shown in Figure 5. The ground state of W_3O_{10} possesses C_1 (^1A) symmetry (Figure 5a) and can be viewed as replacing a terminal O atom in W_3O_9 by an O_2 unit. A triplet isomer without the O_2 unit is 1.25 eV higher in energy (Figure 5b). This isomer, however, becomes the ground state for the $W_3O_{10}^-$ anion (Figure 5c), whereas the isomer with the O_2 unit is significantly higher by 1.57 eV in the anion (Figure 5d).

5. Discussion

5.1. Comparisons between Experimental and Theoretical Results and Interpretation of the Photoelectron Spectra. Photodetachment involves removal of electrons from occupied molecular orbitals (MOs) of the anions. The final states of the electron detachment are the electronic ground and excited states of the corresponding neutrals. The differences between the higher-binding energy bands and the lowest-binding energy band in an anion photoelectron spectrum represent the excitation energies of the neutral cluster. The simulated spectra of the whole $W_3O_n^-$ ($n = 7-10$) series are shown in Figure 6. All the calculated VDEs are given in Table 1 along with the experimental data.

Within the one-electron formalism, each occupied MO for a closed-shell anion will generate a single PES band with the associated vibrational structures governed by the Franck—Condon principle. However, all the $W_3O_n^-$ anions are open shell with a single unpaired electron in their lowest energy structures. In these cases, detachment from a fully occupied MO would result in two detachment channels due to the removal of either the spin-down (β) or the spin-up (α) electrons, giving rise to triplet (T) and singlet (S) final states, respectively, as given in Table 1.

5.1.1. $W_3O_9^-$. The valence electron configuration of W_3O_9 ($^1A_1'$, D_{3h}) is $(6e'')^4(12e')^4(7e'')^4$ $(6a_2'')^2$, all of which are primarily O 2p-based orbitals. In $W_3O_9^-$ the extra electron enters the $10a_1'$ LUMO of W_3O_9, resulting in a doublet ($^2A_1'$) state for the anion. The calculated spin densities indicate that the extra electron is equally shared by the three W atoms. The three-dimensional contour of the $10a_1'$ MO is shown in Figure 7,

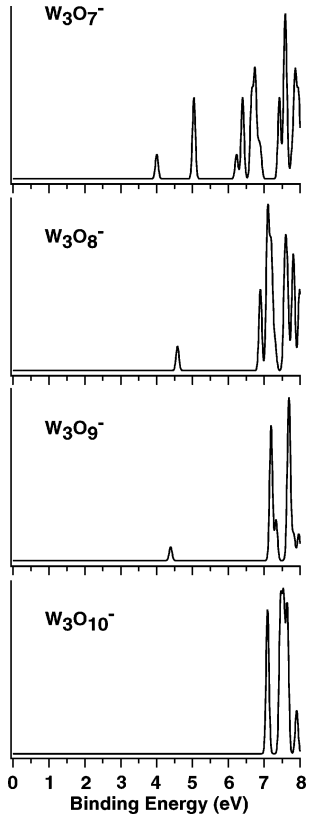

Figure 6. Simulated photoelectron spectra of $W_3O_n^-$ ($n = 7-10$). The simulated spectra were based on the optimized anion ground-state structures (Figures 2−5) and were constructed by fitting the distribution of the calculated vertical detachment energies (Table 1) with unit-area Gaussian functions of 0.04 eV full width at half maximum.

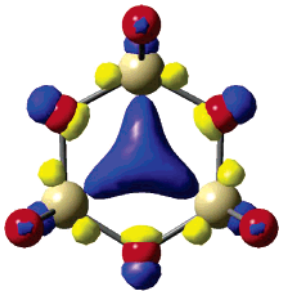

Figure 7. The HOMO picture of $W_3O_9^-$.

which is a one-electron three-center metal−metal bond.[25] This bond pulls the three W atoms closer in the anion, resulting in a nearly perfect W_3O_3 hexagon in $W_3O_9^-$ (Figure 2). The broad PES band for the ground-state transition (X, Figure 1c) is in excellent agreement with the large geometry changes upon detachment of the $10a_1'$ electron in $W_3O_9^-$. The calculated VDE of 4.39 eV (Table 1) for this detachment channel compares well with the experimental VDE at ∼4.2 eV. As shown in Table 1, the calculated VDE for detachment from the first primarily O 2p-type MO, $6a_2''$ (corresponding to the HOMO of neutral W_3O_9), is 7.18 eV, followed immediately by the detachment from the doubly degenerate 7e″ MO with a calculated VDE of 7.20 eV. A total of 8 detachment channels are calculated up to 7.8 eV for the O 2p-type orbitals (Table 1). This high density of electronic states from the O 2p-type MOs and their calculated VDEs are in good agreement with the continuous spectral features observed in the high binding energy part of the photoelectron spectrum (Figure 1c).

5.1.2. $W_3O_8^-$. The ground state of W_3O_8 is the tribridged C_s structure (Figure 3a), with the dibridged C_{2v} structure (Figure 3b) being 0.46 eV higher in energy. There is a competition between W−W and W−O bonding. In the C_s structure, there is no W−W bonding, and the extra pair of d electrons is essentially a lone pair localized on the tricoordinated W atom, as shown in Figure 8a. On the other hand, there is a direct W−W bond in the C_{2v} structure, which becomes the ground state in the anion (Figure 3c) with a valence-electron configuration of $(6a_2)^2(14b_2)^2(11b_1)^2(12b_1)^2(7a_2)^2(18a_1)^2(19a_1)^1$, where the extra electron enters the $19a_1$ orbital with d−d π-bonding character (Figure 8b). The $18a_1$ MO is a d−d σ-bonding orbital (Figure 8b), and all MOs from $7a_2$ and below are of O 2p character.

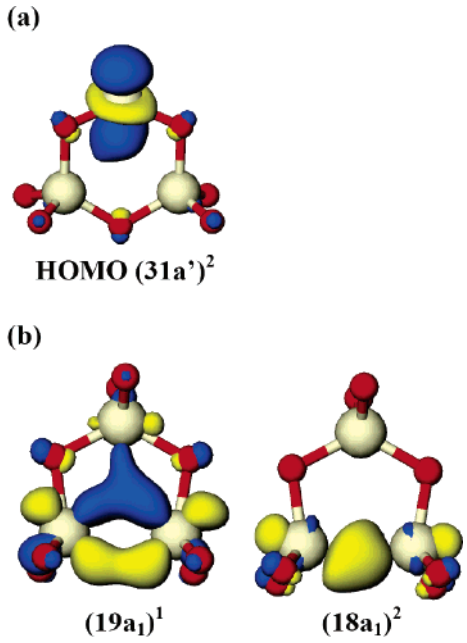

Figure 8. (a) The HOMO picture for the ground state of W_3O_8 (Figure 3a). (b) The top two molecular orbitals of the $W_3O_8^-$ anion (Figure 3c).

Photodetachment from the singly occupied $19a_1$ orbital of $W_3O_8^-$ yields the first PES band X (VDE: 4.62 eV), which is in excellent agreement with the calculated VDE of 4.58 eV (Table 1). The next detachment channel is from $18a_1(\beta)$ with a calculated VDE of 6.89 eV, in excellent agreement with band A (VDE = 6.78 eV) (Figure 1b). The calculated VDE from $18a_1(\alpha)$ is 7.59 eV, which falls in the spectral region where detachments from O 2p-based MOs dominate (Table 1). As shown in Table 1, band B in the photoelectron spectrum can be assigned to electron detachment transitions from the MO group ($7a_2$, $12b_1$, $11b_1$). The calculated VDEs for detachment from $14b_2(\beta)$ and $6a_2(\beta)$ are 7.58 and 7.64 eV, respectively, in good agreement with band C (VDE: 7.65 eV). Overall the calculated VDEs from the $W_3O_8^-$ anion ground state are in excellent agreement with the observed PES spectra. We should point out that the calculated VDEs for the tri-bridged C_s isomer of $W_3O_8^-$ are much lower and disagree with the observed photoelectron spectral features.

5.1.3. $W_3O_7^-$. The W_3O_7 and $W_3O_7^-$ species represent the most complicated systems in our current study, primarily because of competitions between the W−W, W−O, and W═O bonding. The two low-lying structures of W_3O_7 (Figure 4a, b) have very different W−O connectivities, but surprisingly they are nearly degenerate in energy, with the tribridged structure (Figure 4a) being slightly more stable. Molecular orbital analysis shows that the ground state of W_3O_7 involves π-bonding and antibonding interactions in its HOMO and LUMO, respectively, as shown in Figure 9a.

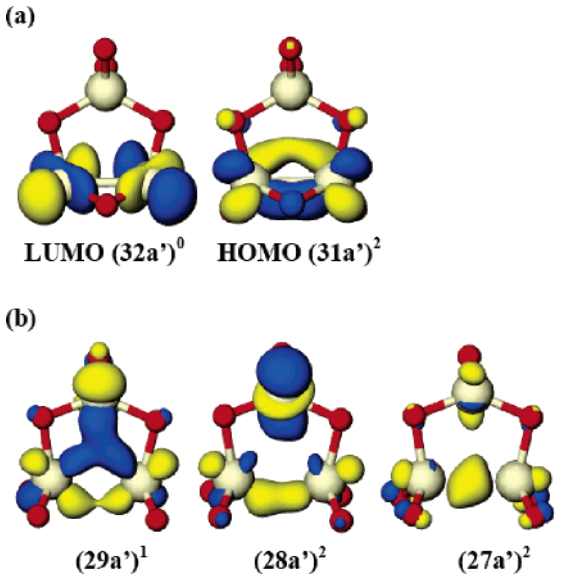

Figure 9. (a) LUMO and HOMO pictures of the tribridged W_3O_7 neutral (Figure 4a). (b) The molecular orbitals of the $W_3O_7^-$ anion (Figure 4e).

In the $W_3O_7^-$ anion, the dibridged isomer becomes the global minimum (Figure 4e), with the tribridged isomer being 0.10 eV higher in energy. The dibridged $W_3O_7^-$ cluster has C_s (^{2}A′) symmetry with an electron configuration of (25a′)^2(20a″)^2(26a′)^2-(21a″)^2(27a′)^2(28a′)^2(29a′)^1. The extra electron in the anion enters the 29a′ orbital (Figure 9b), which is a three-center W−W bonding orbital. This is why the dibridged isomer is more stable than the tribridged isomer in the anion because the LUMO of the latter is an antibonding orbital (Figure 9a). The 28a′ and 27a′ MOs are also primarily W−W bonding orbitals (Figure 9b), and all other MOs below 27a′ are O 2p-type orbitals. Detachment from the 29a′ orbital results in the X band in the photoelectron spectrum of $W_3O_7^-$. The calculated VDE of 4.01 eV (Table 1) is in good agreement with the experimental VDE of the X band (3.90 eV). The next transition is from 28a′(β) with a calculated VDE of 5.04 eV, which is in excellent agreement with band A (VDE: 5.04 eV). Overall the calculated VDEs from the dibrided $W_3O_7^-$ isomer agree well with the main PES spectral features, as shown in Figure 10.

However, the tribridged isomer is very close in energy to the dibridged isomer in both the neutral and the anion and would give a similar VDE for the ground-state transition. Thus, we also calculated the VDEs and simulated the spectrum from the tribridged isomer, as compared with the experimental spectrum and that from the dibridged isomer in Figure 10. Even though the first calculated detachment transition of the tribridged isomer is also very close to the X band of the experimental spectrum, the overall PES pattern of the tribridged isomer disagree with the main features of the experimental spectrum. We note that the tribridged isomer may have minor contributions to the observed spectrum. For example, the shoulder on the lower binding energy side of band A may come from the second band of the tribridged isomer. The congested spectral features in the higher binding energy part of the spectrum above 6 eV also indicate that there may be contributions from both isomers. These observations illustrate the sensitivity of the photoelectron spectrum to the cluster structures, lending credence to the dibridged $W_3O_7^-$ isomer as the global minimum.

5.1.4. $W_3O_{10}^-$. The ground state of W_3O_{10} is a closed-shell C_1 (^{1}A) species with an O_2 unit (Figure 5a). The HOMO of this cluster corresponds to the π^* orbital of the O−O moiety,

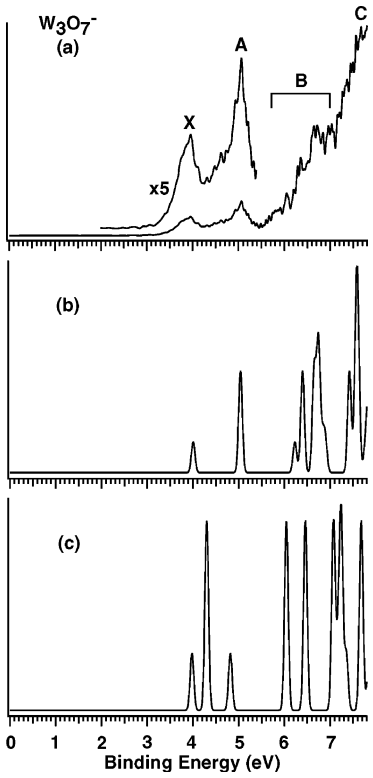

Figure 10. Comparison of the $W_3O_7^-$ photoelectron spectrum (a) with the simulated spectra from the global minimum dibridged isomer (b) and the tribridged isomer (c).

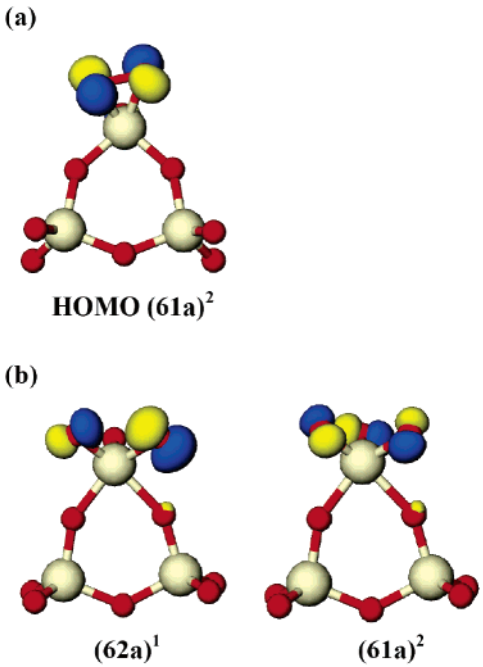

Figure 11. (a) The HOMO picture of neutral W_3O_{10}. (b) The molecular orbitals of the $W_3O_{10}^-$ anion.

as shown in Figure 11a. Addition of an electron into the π^* orbital in the anion completely breaks the O−O bond in the ground state of $W_3O_{10}^-$ (Figure 5c). The isomer with the O−O unit (Figure 5d), in which the extra electron occupies a higher-lying W 5d type orbital, is much higher in energy by 1.57 eV. The ground state of $W_3O_{10}^-$ has an electron configuration of (57a)^2(58a)^2(59a)^2(60a)^2(61a)^2(62a)^1. All MOs are of O 2p character; the 62a and 61a MOs are derived from the σ^* and π^* of the O_2 unit, respectively, as shown in Figure 11b.

The $W_3O_{10}^-$ anion has very high electron binding energies, and all detachment transitions occur above 7 eV (Figure 1d). Thus only a very narrow spectral range was observed at 157 nm without any resolved features. The calculated VDE from detachment from the 62a HOMO of $W_3O_{10}^-$ is 7.09 eV, in excellent agreement with the observed onset of the photoelectron spectrum. Several other detachment channels are within the 157 nm photon energies, as shown in Table 1.

5.2. W_3O_9: The Smallest Cluster as Molecular Models for Bulk Tungsten Oxide. W_3O_9 is a stoichiometric molecule and has been observed to be a major species in the vapor phase of tungsten oxide.[26,27] The large HOMO−LUMO gap observed in our PES spectrum is consistent with the fact that W_3O_9 should be a relatively stable molecule. Each W in W_3O_9 is tetrahedrally coordinated with four O atoms and is chemically saturated, i.e., all W atoms are in the maximum W^{6+} oxidation state and O atoms are in their maximum O^{2-} oxidation state. The bridging W−O bonds are single bonds, whereas the terminal O atoms form W═O double bonds. Importantly, we observed that the HOMO−LUMO gap of W_3O_9 is ∼3.4 eV, which already reaches that of bulk WO_3 (indirect gap, ∼2.6 eV; direct gap, ∼3.5−3.7 eV).[45] Previously, we measured that WO_3 molecule has a HOMO−LUMO gap of 1.4 eV,[21] which increases to 2.8 eV in W_2O_6.[24] It is known that WO_3 has a monoclinic lattice at room temperature. The bulk structure of WO_3 is composed of corner sharing WO_6 octahedra in a ReO_3-like framework with tilting and distortions of the octahedral, giving structures with lower symmetry than the ideal cubic structure.[46] The calculated bridging W−O bond length in the W_3O_9 is 1.91 Å, which is very close to the bulk value of 1.90 Å. The W−W distance in the W_3O_9 cluster is 3.55 Å, while it is ∼3.7 Å in the bulk WO_3. In addition, the calculated W═O vibrational frequencies of the W_3O_9 cluster are quite close to those of terminal W═O from the surface Raman measurements.[47] The unscaled B3LYP Raman band for W═O in W_3O_9 lies at ∼1038−1043 cm^{-1}, while the surface W═O band is at 950 cm^{-1}. Thus, the W_3O_9 cluster is the smallest species that can be considered as a molecular model for bulk WO_3 from an electronic structure and chemical point of view.

5.3. Chemical Bonding in Nonstoichiometric W_3O_n Clusters: W_3O_8 as a Molecular Model for O-Deficient Defect Sites. The structure of W_3O_{10} with an O_2 unit is interesting and is consistent with our previous finding on O-rich oxide clusters. We have found that in O-rich oxide clusters O_2 unit can replace an O atom.[21,48,49] Thus, W_3O_{10} can be viewed as replacing a terminal O atom in the D_{3h} W_3O_9 by an O_2 unit. The O-deficient clusters are more complicated. It appears that there is a competition between W−O single bond and W═O double bond. In the tribridged W_3O_8 global minimum (Figure 3a), there are five terminal W═O units, whereas in the dibridged low-lying isomer (Figure 3b), there are six terminal W═O units. Clearly, two bridging W−O single bonds in the former are favored over the W═O double bond in the latter. In W_3O_7, a similar competition exists among the low-lying isomers (Figure 4). Again, the tribridged isomer (Figure 4a) with the most bridging W−O bonds is favored.

The global minimum of W_3O_8 (Figure 3a) is formed by removing a terminal O atom from the stoichiometric W_3O_9 cluster, creating a tricoordinated W site. Our MO analysis shows that this W site has a pair of localized d electrons (Figure 8a) and it is essentially a localized W^{4+} site. Such defect sites are chemically active and may act as catalytic centers in bulk oxides or catalysts.[22] For example, the localized d electrons on the W^{4+} site may be readily transferred to the π^* orbitals of an approaching O_2 molecule, making W_3O_8 a molecular model for O_2 activation. In fact, the O-rich W_3O_{10} cluster can be viewed exactly as the product of W_3O_8 reacting with a O_2 molecule

$$W_3O_8 + O_2 \rightarrow W_3O_{10}\ (-78\ \text{kcal/mol}\ (-3.4\ \text{eV})) \quad (1)$$

Our calculation yielded an O_2 chemisorption energy of −78 kcal/mol to the W^{4+} defect site in W_3O_8. The O−O distance (1.49 Å) in W_3O_{10} (Figure 5a) is much longer than that in free O_2 and is close to that in peroxo O_2^{2-}. We expect that the W_3O_8 cluster can activate other molecules, as well, and may be considered as a molecular model for O-deficient defect sites in tungsten oxides.

6. Conclusions

We report a systematic photoelectron spectroscopy and density functional study of a series of tri-tungsten oxide clusters: $W_3O_n^-$ and W_3O_n ($n = 7-10$). Detachment features due to W 5d and O 2p features were observed in $W_3O_7^-$ and $W_3O_8^-$ with the 5d feature at lower electron binding energies and the O 2p features at very high electron binding energies. A large energy gap was observed in the photoelectron spectrum of $W_3O_9^-$, yielding a HOMO−LUMO gap of ∼3.4 eV for the stoichiometric W_3O_9 molecule. High electron binding energies (>7.0 eV) were observed for $W_3O_{10}^-$, suggesting that the W_3O_{10} neutral cluster is an unusually strong oxidizing agent. Extensive density functional calculations were carried out and combined with the experimental data to elucidate the geometries, electronic structures, and chemical bonding in the W_3O_n clusters. Our calculations show that W_3O_9 is a D_{3h} cluster with a W_3O_3 six-membered ring and two terminal W═O units on each W site. The structure of W_3O_8 can be viewed as removing a terminal O atom from W_3O_9, whereas that of W_3O_7 can be viewed as removing two terminal O atoms from W_3O_9. The O-rich cluster W_3O_{10} can be viewed with replacing a terminal O atom in W_3O_9 by an O_2 unit. The W_3O_8 cluster thus contains a tricoordinated W site, which is found to possess a pair of localized 5d electron and is a localized W^{4+} defect site. It is shown that this defect site can readily react with O_2 to form W_3O_{10} with a −78 kcal/mol O_2 chemisorption energy. It is suggested that W_3O_8 can be considered as a model for O-deficient defect sites in tungsten oxides.

Acknowledgment. We thank Dr. B. Kiran for valuable discussions. This work was supported by the Chemical Sciences, Geosciences and Biosciences Division, Office of Basic Energy Sciences, U.S. Department of Energy (DOE) under Grant No. DE-FG02-03ER15481 (Catalysis Center Program) and was performed at the W. R. Wiley Environmental Molecular Sciences Laboratory (EMSL), a national scientific user facility sponsored by the DOE's Office of Biological and Environmental Research and located at Pacific Northwest National Laboratory, operated for DOE by Battelle. All calculations were performed using the EMSL Molecular Science Computing Facility.

References and Notes

(1) Manno, D.; Serra, A.; Giulio, M. D.; Micocci, G.; Tepore, A. *Thin Solid Films* **1998**, *324*, 44.

(2) Moulzolf, S. C.; LeGore, L. J.; Lad, R. J. *Thin Solid Films* **2001**, *400*, 56.

(3) Granqvist, C. G. *Solar Energy Mater. Solar Cells* **2000**, *60*, 201.

(4) Bessiere, A.; Marcel, C.; Morcrette, M.; Tarascon, J. M.; Lucas, V.; Viana, B.; Baffier, N. *J. Appl. Phys.* **2002**, *91*, 1589−1594.

(5) Salvatl, L., Jr.; Makovsky, L. E.; Stencel, J. M.; Brown, F. R.; Hercules, D. M. *J. Phys. Chem.* **1981**, *85*, 3700.

(6) Horsley, J. A.; Wachs, I. E.; Brown, J. M.; Via, G. H.; Hardcastle, F. D. *J. Phys. Chem.* **1987**, *91*, 4014.
(7) Gazzoli, D. Valigi, M.; Dragone, R.; Marucci, A.; Mattei, G. *J. Phys. Chem. B* **1997**, *101*, 11129.
(8) Bigey, C.; Hilaire, L.; Maire, G. *J. Catal*. **2001**, *198*, 208.
(9) Ji, S. F.; Xiao, T. C.; Li, S. B.; Xu, C. Z.; Hou, R. L.; Coleman, K. S.; Green, M. L. H. *Appl. Catal. A* **2002**, *225*, 271.
(10) Mamede, A. S.; Payen, E.; Grange, P.; Poncelet, G.; Ion, A.; Alifanti, M.; Parvulescu, V. I. *J. Catal*. **2004**, *223*, 1.
(11) Weinstock, I. A.; Barbuzzi, E. M. G.; Wemple, M. W.; Cowan, J. J.; Reiner, R. S.; Sonnen, D. M.; Heintz, R. A.; Bond, J. S.; Hill, C. L. *Nature*. **2001**, *414*, 191.
(12) Zemski, K. A.; Justes, D. R.; Castleman, A. W., Jr. *J. Phys. Chem. B* **2002**, *106*, 6136
(13) Fialko, E. F.; Kirkhtenko, A. V.; Goncharov, V. B.; Zamaraev, K. I. *J. Phys. Chem. B* **1997**, *101*, 5772. (b) Vyboishchikov, S. F.; Sauer, J. *J. Phys. Chem. A* **2001**, *105*, 8588. (c) Tenorio, F. J.; Murray, I.; Martinez, A.; Klabunde, K. J.; Ortiz, J. V. *J. Chem. Phys*. **2004**, *120*, 7955. (d) Asmis, K. R.; Santambrogio, G.; Brümmer, M.; Sauer, J. *Angew. Chem., Int. Ed*. **2005**, *44*, 3122. (e) Böhme, D. K.; Schwarz, H. *Angew. Chem., Int. Ed*. **2005**, *44*, 2336.
(14) Waters, T.; O'Hair, R. A.; Wedd, A. G. *J. Am. Chem. Soc*. **2003**, *125*, 3384.
(15) Socaciu, L. D.; Hagen, J.; Bernhardt, T. M.; Woste, L.; Heiz, U.; Hakkinen, H.; Landman, U. *J. Am. Chem. Soc.* **2003**, *125*, 10437.
(16) Jackson, P.; Fisher, K. J.; Willett, G. D. *Chem. Phys.* **2000**, *262*, 179.
(17) Asmis, K. R.; Brümmer, M.; Kaposta, C.; Santambrogio, G.; von Helden, G.; Meijer, G.; Rademann, K.; Woste, L. *Phys. Chem. Chem. Phys.* **2002**, *4*, 1101.
(18) Shi, Y.; Ervin, K. M. *J. Chem. Phys.* **1998**, *108*, 1757.
(19) (a) Justes, D. R.; Mitrić, R.; Moore, N. A.; Bonačič-Koutecký, V.; Castleman, A. W., Jr. J. Am. Chem. Soc. **2003**, *125*, 6289. (b) Fielicke, A.; Mitri'c, R.; Meijer, G.; Bonačič-Koutecký, V.; von Helden, G. *J. Am. Chem. Soc*. **2003**, *125*, 15716. (c) Asmis, K. R.; Meijer, G.; Brümmer, M.; Kaposta, C.; Santambrogio, G.; Wöste, L.; Sauer, J. *J. Chem. Phys*. **2004**, *120*, 6461. (d) Fielicke, A.; Meijer, G.; Helden, G. v. *J. Am. Chem. Soc*. **2003**, *125*, 3659.
(20) Yoder, B. L.; Maze, J. T.; Raghavachari, K.; Jarrold, C. C. *J. Chem. Phys.* **2005**, *122*, 094313.
(21) Zhai, H. J.; Kiran, B.; Cui, L. F.; Li, X.; Dixon, D. A.; Wang, L. S. *J. Am. Chem. Soc*. **2004**, *126*, 16134.
(22) Jang, Y. H.; Goddard, W. A., III *J. Phys. Chem. B* **2002**, *106*, 5997.
(23) Fu, G.; Xu, X.; Lu, X.; Wan, H. *J. Am. Chem. Soc.* **2005**, *127*, 3989.
(24) Zhai, H. J.; Huang, X.; Cui, L. F.; Li, X.; Li, J.; Wang, L. S. *J. Phys. Chem. A* **2005**, *109*, 6019.
(25) Huang, X.; Zhai, H. J.; Kiran, B.; Wang, L. S. *Angew. Chem., Int. Ed*. **2005**, *44*, 7251.
(26) Berkowitz, J.; Chupka, W. A.; Inghram, M. G. *J. Chem. Phys*. **1957**, *27*, 85.
(27) Azens, A.; Kitenbergs, M.; Kanders, U. *Vacuum* **1995**, *7*, 745.
(28) Weltner, W., Jr.; MeLeod, D., Jr. *J. Mol. Spect*. **1965**, *17*, 276.
(29) Sun, Q.; Rao, B. K.; Jena, P.; Stolcic, D.; Kim, Y. D.; Gantefor, G.; Castleman, A. W., Jr. *J. Chem. Phys*. **2004**, *121*, 9417.
(30) Wang, L.S.; Cheng, H. S.; Fan, J. *J. Chem. Phys*. **1995**, *102*, 9480.
(31) Wang, L. S.; Wu, H. In *Advances in Metal and Semiconductor Clusters. IV. Cluster Materials*; Duncan, M. A., Ed.; JAI: Greenwich, CT, 1998; pp 299−343.
(32) Becke, A. D. *J. Chem. Phys*. **1993**, *98*, 1372.
(33) Lee, C.; Yang, W.; Parr, R. G. *Phys. Rev. B* **1988**, *37*, 785.
(34) Stephens, P. J.; Devlin, F. J.; Chabalowski, C. F.; Frisch, M. J. *J. Phys. Chem*. **1994**, *98*, 11623.
(35) Andrae, D.; Haeussermann, U.; Dolg, M.; Stoll, H.; Preuss, H. *Theor. Chim. Acta* **1990**, *77*, 123.
(36) Küchle, W.; Dolg, M.; Stoll, H.; Preuss, H. *Pseudopotentials of the Stuttgart/Dresden Group 1998*, revision August 11, 1998; http://www.theochem.uni-stuttgart.de/pseudopotentiale.
(37) Martin, J. M. L.; Sundermann, A. *J. Chem. Phys*. **2001**, *114*, 3408.
(38) Dunning, T. H., Jr. *J. Chem. Phys*. **1989**, *90*, 1007.
(39) Kendall, R. A.; Dunning, T. H., Jr.; Harrison, R. J. *J. Chem. Phys*. **1992**, *96*, 6796.
(40) Yang, X.; Waters, T.; Wang, X. B.; O'Hair, R. A. J.; Wedd, A. G.; Li, J.; Dixon, D. A.; Wang, L. S. *J. Phys. Chem. A* **2004**, *108*, 10089.
(41) Li, J.; Li, X.; Zhai, H. J.; Wang, L. S. *Science* **2003**, *299*, 864.
(42) Li, X.; Kiran, B.; Li, J.; Zhai, H. J.; Wang, L. S. *Angew. Chem., Int. Ed*. **2002**, *41*, 4786.
(43) *NWChem, A Computational Chemistry Package for Parallel Computers, Version 4.6*; Pacific Northwest National Laboratory: Richland, WA, 2004.
(44) Extensible Computational Chemistry Environment, http:// ec-ce.emsl.pnl.gov/.
(45) Koffyberg, F. P.; Dwight, K.; Wold, A. *Solid State Commun*. **1979**, *30*, 433.
(46) Salje, E. K. H.; Rehman, S.; Pobell, F.; Morris, D.; Knight, K. S.; Herrmannsdörfer, T.; Dove, M. T. *J. Phys.: Condens. Matter* **1997**, *9*, 6563. (b) Jones, F. H.; Rawlings, K.; Foord, J. S.; Cox, P. A.; Egdell, R. G.; Pethica, J. B.; Wanklyn, B. M. R. *Phys. Rev. B* **1995**, *52*, 14392.
(47) Cazzanelli, E.; Mariotto, G.; Vinegoni, C.; Kuzmin, A.; Purans, J. *Proc. Electrochem. Soc.* **1996**, *96*, 1199.
(48) Zhai, H. J.; Wang, L. S. *J. Chem. Phys*. **2002**, *117*, 7882.
(49) Wu, H.; Desai, S. R.; Wang, L. S. *J. Am. Chem. Soc*. **1996**, *118*, 5296.